AIAA JOURNAL
Vol. 48, No. 7, July 2010

Structural Health Monitoring Sensor Placement Optimization Under Uncertainty

Robert F. Guratzsch* and Sankaran Mahadevan†
Vanderbilt University, Nashville, Tennessee 37235

DOI: 10.2514/1.28435

This paper develops a methodology for the optimum layout design of sensor arrays of structural health monitoring systems under uncertainty. This includes finite element analysis under transient mechanical and thermal loads and incorporation of uncertainty quantification methods. The finite element model is validated with experimental data, accounting for uncertainties in experimental measurements and model predictions. The structural health monitoring sensors need to be placed optimally in order to detect with high reliability any structural damage before it turns critical. The proposed methodology achieves this objective by combining probabilistic finite element analysis, structural damage detection algorithms, and reliability-based optimization concepts.

Nomenclature

a	=	number of optimal sensor locations
D	=	observed difference between model prediction and experimental observation
$d_j(x)$	=	discriminant function of structural state j (i.e. Mahalanobis distance)
$F(t)$	=	temperature scale factor for Young's modulus
$f(x)$	=	objective function
$g_o(x_1, x_2, \phi)$	=	Gaussian random field
N_{opt}	=	number of features most effective for state classification
n	=	number of candidate sensor locations
n_d	=	number of data points used to calculate $\bar{x}$ and s
$P(CD)$	=	probability of correct detection
$S(\omega_{k_i})$	=	two-sided spectral density function of $g_o(x_1, x_2, \phi)$
t	=	temperature of test article (degrees Fahrenheit)
$[u, v]$	=	bounded box that contains all possible x (i.e. geometric constraints on x)
μ_j, Σ_j	=	mean feature vector and covariance matrix of the learning data set of structural state j
x	=	vector containing the coordinates of a given sensor array
$\bar{x}$, s	=	sample mean and sample standard deviation of model predictions
x^{best}	=	optimal sensor array
ε	=	sufficiently small value
σ_{vM}	=	equivalent von Mises stress
σ_x, σ_y, τ_{xy}	=	in-plane stress components
$\Phi[\cdot]$	=	cumulative distribution function of the standard normal distribution
$\{\Psi_A\}$	=	analytically predicted mode shape vector
$\{\Psi_X\}$	=	experimentally measured mode shape vector

Presented as Paper 7034 at the 11th AIAA/ISSMO Multidisciplinary Analysis and Optimization Conference, Portsmouth, Virginia, 6–8 September 2006; received 19 October 2006; revision received 16 December 2007; accepted for publication 31 January 2008.

*Graduate Student, Civil and Environmental Engineering Department, VU Station B 351831, 2301 Vanderbilt Place.

†Professor of Civil and Environmental Engineering, VU Station B 351831, 2301 Vanderbilt Place. Senior Member AIAA.

I. Introduction

STRUCTURAL health monitoring (SHM) systems that report in real-time the flight vehicle's condition in terms of reactions, stresses, and displacements, are central to meeting the demanding goals of increasing flight vehicle safety and reliability, while reducing vehicle operating and maintenance costs [1]. The SHM system must be small, lightweight, energy efficient, and the most reliable subsystem onboard the flight structure in order to make incorporation into existing flight vehicle designs possible with minimal impact on the structure's performance. The structural behavior prediction of next generation flight vehicles, such as the space operations vehicle, has uncertainty due to the uncertainties in the flight environment and loads, geometry, material properties, etc. A probabilistic structural analysis that includes these various sources of uncertainty is vital toward the success of the structural health assessment. This includes the development of a finite element model, uncertainty quantification methods, and optimization techniques. Additionally, in order for the SHM system to detect with maximum probability any structural damage before it becomes critical, SHM system sensors need to be optimally placed. While many advances have been made in terms of sensor technology, damage detection algorithms, structural reliability, and deterministic sensor placement optimization (SPO) schemes, additional research needs to be focused on probabilistic modeling in the context of SHM, as well as on SPO under uncertainty, in order to maximize the reliability of the structural condition assessment while taking the various sources of uncertainty into account.

This paper develops a methodology for integrating the advances in various individual disciplines for the optimum design of SHM system sensor arrays under uncertainty. The methodology aims at maximizing the reliability of damage detection by designing the locations of SHM system sensors. This includes the following steps: 1) structural simulation and model validation, 2) probabilistic analysis, 3) damage detection, and 4) SPO. The proposed framework is general, but the selection of methods within each of the above four steps can be tailored to different applications and sensing techniques. In this paper, steps 1 and 2 focus on combining finite element analysis and probabilistic analysis to estimate the variability of structural response. Step 3 focuses on vibration-based methods, making use of modal parameters and vibration signal features (in time or frequency domains). Step 4 focuses on the optimization of locations of a fixed number of sensors on a two-dimensional layout, in order to maximize the reliability of the damage detection. Depending on the application problem, different sensing techniques and damage detection algorithms may be preferable in step 3, and different optimization techniques may be preferable in step 4. Also in step 4, some application problems may need to consider the number of sensors as an additional optimization variable. Section II of this paper defines the general methodology, while Sec. III provides a numerical example to

demonstrate SPO under uncertainty for a prototype of a thermal protection system panel where damage detection is with respect to loose bolts.

II. Previous Work

Several studies have investigated SPO during recent years. Hiramoto et al. [2] as well as Abdullah et al. [3] have addressed the need to place actuators in an optimal way to control the behavior of dynamic structures, where Hiramoto et al. uses the explicit solution of the algebraic Riccati equation to determine the optimal actuator placement and Abdullah et al. utilizes genetic algorithms (GA) to solve the optimization. GA have also been employed to search for optimal locations of actuators in active vibration control [4–7]. With respect to SHM, Guo et al. [8] use a GA approach and a SPO performance index based on damage detection to search for an optimal sensor array and Spanache et al. [9] use GA and account for economic/cost issues in the design of a cost optimal sensor system. However, GA-based sensor/actuator placement optimization methods often generate invalid strings during the evolution process and require a predefined number of discrete sensor configurations, which do not guarantee global optima.

Additionally, terrorism concerns have recently caused an increased interest in using sensor arrays for monitoring potential attacks on municipal water distribution systems [10]. In this context, SPO has been attempted with respect to different objectives: population exposed, volume of contaminated water consumed, and time to detection [11]. However, Watson et al. [12] point out that in practice a multi-objective optimization, which simultaneously considers multiple performance measures is more appropriate. Other research areas that have shown a need for sensor networks and SPO include environmental monitoring (algae biomass monitoring, light intensity monitoring, etc.) [13,14] monitoring of spatial distributions [15] and military surveillance operations [16]. In all of these methodologies, a predefined number of discrete sensor locations from which the sensor networks grow must be provided.

Related more closely to SPO of SHM systems of next generation flight vehicles, Li et al. [17] proposed an algorithm that aims to identify modal frequencies and mode shapes, as well as increase the signal to noise ratio. However, it is not shown that a sensor array that best identifies modal frequencies and mode shapes optimizes more traditional SHM performance measures such as the probability of correct classification. Gao and Rose [18] define a probabilistic SPO approach, where a probabilistic damage detection model that describes detection probabilities over a confidence monitoring region with radius R is defined for each sensor of a given sensor set. The entire effectiveness of the sensor network is then assumed to be the joint effect of all sensors as estimated at a point by the union probability of all sensors. A covariance matrix adaptation evolution strategy is used to search the decision variable domain. Difficulties arise defining the probabilistic damage detection models and sources for uncertainty are not identified specifically. A similar SPO framework that addresses imprecise detection probabilities as well as uncertain terrain properties is proposed by Dhillon et al. [19]. Parker and Frazier [20] address SPO for SHM based upon the concept of observability from the fields of dynamic systems theory and engineering design optimization. The technique uses a dynamic model of the structure to obtain performance measures with respect to damage detection and localization; however, it does not include uncertainty.

To the authors' best knowledge, the issues due to the spatial and temporal stochastic variability of material, geometric, and loading parameters have not been sufficiently addressed with respect to SPO under uncertainty for SHM systems. The methodology developed in this paper includes the stochastic nature of the model input parameters to perform a probabilistic finite element analysis (utilizing Monte Carlo realizations to derive the statistics of the model outputs). The outputs are used with appropriate damage detection algorithms to estimate probabilistic performance measures of a given sensor layout. Single-objective and multi-objective functions that utilize the probabilistic performance measures individually and in combination are considered. The optimization algorithm considers the individual sensor locations to be the decision variables and combines global and local searches; due to the use of finite element method (FEM), the sensor locations are discrete, at finite element grid points.

III. Proposed Methodology

A. Structural Simulation and Model Validation

For many realistic structures, the response due to various loads cannot be determined via a closed-form function of the input variables. The response must be computed through numerical procedures such as a FEM. Several finite element software packages are available. Regardless of the software package used, structural models and their corresponding simulations must capture the relevant physical phenomena and include the relevant input parameters. The appropriate analysis may include linear, nonlinear, and/or coupled structural–thermal simulations.

In addition, model verification and validation is of extreme importance before employing the model results for damage detection and sensor layout optimization. Several validation metrics have been proposed to asses the predictive capability of models, such as the modal assurance criterion (MAC), the modal scale factor [21], and a newly developed model reliability metric (MRM) [22]. Validation of numerical models by comparison against experimental observations has to account for errors and uncertainties in both model predictions and measured observations. Classical and Bayesian hypothesis testing methods have been used to estimate the confidence in model prediction [22].

B. Probabilistic Analysis

Structural model parameters such as distributed loads and material and geometric properties have temporal and spatial variability and cannot be expressed as single random variables, but must be represented as random processes and random fields [23]. Thus random process/field modeling is a key step in probabilistic finite element analysis. The Karhunen–Loeve expansion (KLE) has been used extensively to simulate Gaussian random processes [24]. The wavelet transform method is an extension of the KLE simulation algorithm and is applicable to nonstationary Gaussian processes and fields. Other random process/field generation sequences include the Pierson–Moskowitz Wave Spectra, the JONSWAP spectra [25], Sakamoto's polynomial chaos decomposition [26], and Shinozuka's Gaussian stochastic process formulation [27]. For example, the Gaussian stochastic fields and processes in Fig. 1 were generated using Shinozuka's spectral representation formulation and the Wiener–Khinchine relations. Random field realizations, such as the ones shown can be used to simulate component thickness, material moduli, and spatially distributed loads such as thermal and pressure loading. Representing spatially or temporally distributed model inputs through discretized random process/field realizations allows the inclusion of their uncertainty in FEM analyses.

Once the model input parameters are randomly generated via the discretization of random processes/fields and applied as inputs to FEM models, repeated simulations of the finite element analysis at each realization are used to generate statistical and/or sensitivity information on model outputs at each possible sensor location i. For practical purposes, each node of the FEM model may represent a possible sensor location.

C. Damage Detection Algorithms

Damage detection and location identification algorithms that are based on vibration data include wavelet-based approaches [28], modal frequency analysis [29] etc. Property matrix updating, nonlinear response analysis, and damage detection using neural networks are all methods used to manipulate the information gathered by SHM systems for decision making. However, most structural damage detection methods and algorithms found in the literature examine the changes in the measured structural vibration response and analyze the modal frequencies, mode shapes, and

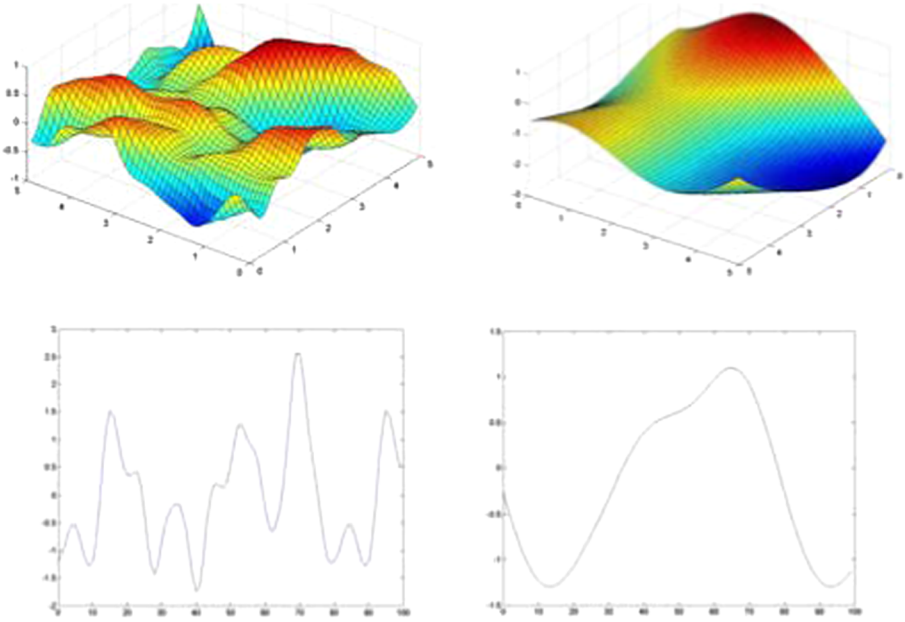

Fig. 1 Random field and process realizations with varying correlation structures.

flexibility/stiffness coefficients of the structure [30]. This can be achieved either actively or passively, where active damage detection algorithms utilize the system response to an auxiliary excitation and passive methodologies utilize only the responses to operational vibrations. A comprehensive review of damage detection and location identification algorithms that use vibration data is provided in [30]. It should be noted that other types of algorithms are useful with other sensing approaches such as eddy-current [31], wave propagation [32], and ultrasonic-acoustic [33] techniques. While the proposed methodology focuses on implementation with respect to vibration-based techniques, the proposed framework itself in terms of assessing the reliability of damage detection, and sensor location optimization to maximize the reliability is quite general. However, specific algorithms will need to be investigated in combination with other sensing approaches.

The probabilistic FEM analysis in the previous section quantifies the statistics of the model outputs at all possible sensor locations. Additional analysis is needed to estimate the probability of correctly identifying the structural state of a component for a given sensor layout, x (i.e. $P(CD) = P(\text{correct structural classification}|\text{ sensor layout } x)$). This can be accomplished via any appropriate diagnostics signal analysis procedure (i.e. damage detection algorithm). The signal analysis procedure employed in this study follows the general concepts of [34] and utilizes the feature extraction and state classification methodologies defined in [34]. Repeated analyses using different realizations of the random inputs to healthy and damaged structural FEM models and their respective state classification constructs a classification matrix from which several performance measures of the given sensor layout can be estimated. Further details of such a procedure are given in Sec. IV.C.

D. Sensor Placement Optimization

The SPO problem can be generalized as "given a set of n candidate locations, find a locations, where $a \ll n$, which provide the best possible performance" [35] in damage detection. Studies by Padula and Kincaid [35,36], DeSimio et al. [37], and Raich and Liszkai [38] have examined the problems and issues involved with SPO. Integer and combinatorial optimization methods have been used to optimize the placement of actuators for vibration control and noise attenuation. In addition, GA for the optimization of sensor layouts [38] have been proposed. Multivariate stochastic approximation using simultaneous perturbation gradient approximation allows for the inclusion of noise in function evaluations or experimental measurements and has been shown to be efficient for large-dimensional problems [39].

An approach to SPO that includes uncertainty is to employ Snobfit [40] (stable noisy optimization by branch and fit), an optimization scheme that is designed for bound-constrained optimization of noisy objective functions, which are costly to evaluate due to computational or experimental complexity. The major advantage of using Snobfit is that the algorithm does not require a previously determined set of candidate sensor locations, but rather considers the following optimization problem:

$$\min f(x) \qquad \text{s.t.} x \in [u, v] \tag{1}$$

where x (the vector of sensor location coordinates) is continuous and $[u, v]$ is a bounded box in $\Re^n$ with a nonempty interior [41].

The underlying idea of the optimization formulation is to identify a sensor layout, x, that will maximize some performance measure, such as the probability of correctly classifying the structure as either healthy or damaged (i.e. classify the structure as healthy when it is indeed healthy and as damaged when it is damaged). Here x represents a vector containing the coordinates of the SHM sensors for a given layout. From the probabilistic analysis described above and a diagnostics signal analysis procedure, performance measures such as probability of detection can be calculated. This allows the optimization formulation given in Eq. (1) to be utilized, where the objective function can be related to various performance measures [see Eqs. (8–11) below] and $[u, v]$ are the geometric constraints on x given by the physical dimensions of the structure.

IV. Application of Methodology

The proposed methodology is implemented using the following example problem. The structure under consideration is described in detail in [40], and shown in Fig. 2. The test article consists of a heat-resistant, 0.25 in. (6.35 mm)-thick, 12 by 12 in. (0.3048 by 0.3048 m) square aluminum plate, held in place via four 0.25 in. (6.35 mm)-diam bolts located 0.50 in. (12.7 mm) from the edges of the plate.

A. Structural Simulation and Model Validation

The structure under consideration is modeled using the commercial finite element software Ansys [41]. A portion of the FEM model is shown in Fig. 3. Four-noded shell elements (Shell63) and two-noded spring elements (Combin14) are utilized to model the aluminum plate and bolted boundary conditions. Approximately 3300 nodes and 2800 elements comprise the 19,836 degree-of-freedom models. In Fig. 3, the four points located near the corners of the plate simulate the bolted boundary conditions via 48 spring

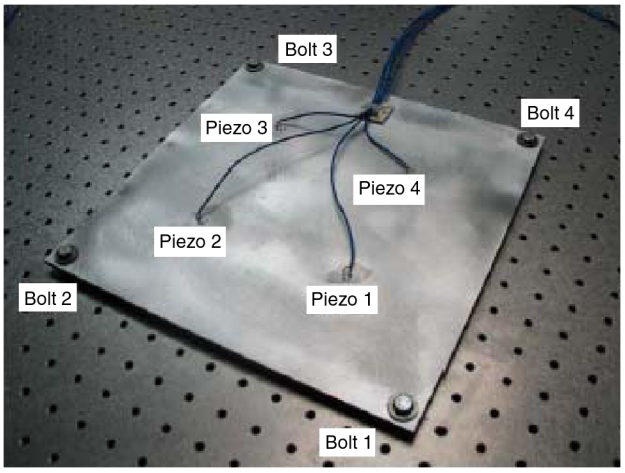

Fig. 2 Experimental setup of aluminum test panel showing bolts and piezoelectric transducer placement [43].

elements per bolt with varying stiffness coefficients (depending on which structural state the model simulates), while the point near the center of the upper left quadrant of the plate simulates the piezoelectric actuator. The analysis is transient and includes a dynamic mechanical load consisting of a sinusoidal frequency sweep, exciting the structure from 0 to 1500 Hz in approximately 2.0 s. This excitation represents the auxiliary input used with active damage detection algorithms. Because of the high frequency of the excitation function, a mode superposition (MSP) transient analysis was used to evaluate the FEM model simulations. MSP analysis sums factored mode shapes, obtained from a modal analysis, to calculate the dynamic response [42]. MSP assumes that the structure behaves linearly.

This study employs two metrics for validation of the finite element model. The MAC [21] provides a measure of the statistical correlation between model predictions and experimental observations. $\{\Psi_X\}$ defines the experimentally measured mode shape vector and $\{\Psi_A\}$ the analytically predicted mode shape vector. MAC is defined as

$$\frac{|\{\Psi_X\}^T \cdot \{\Psi_A\}|^2}{(\{\Psi_X\}^T \cdot \{\Psi_X\})(\{\Psi_A\}^T \cdot \{\Psi_A\})} \tag{2}$$

and is a scalar quantity close to 1.0 if the experimental and theoretical mode shapes are in fact from the same mode. If the two mode shapes, which are being compared, actually relate to two different modes of vibration, a value close to 0.0 should be obtained. Generally speaking, a value in excess of 0.9 implies well correlated modes [21].

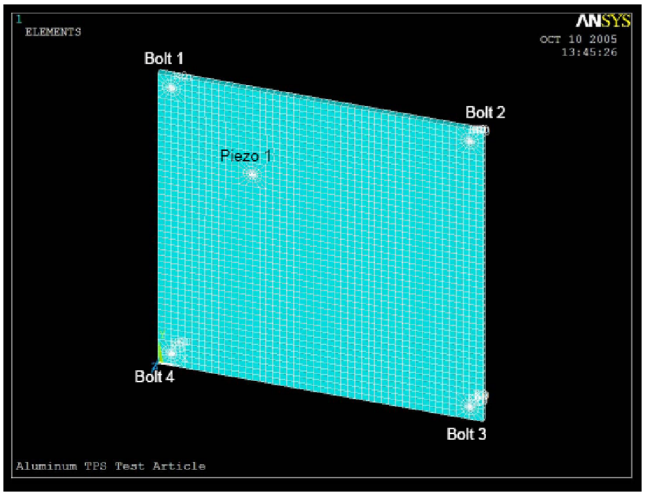

Fig. 3 FEM of test component.

In addition to MAC, Rebba and Mahadevan [22] define a reliability measure via the simple metric $r = P(-\varepsilon < D < \varepsilon)$; i.e., the probability that the observed difference, D, between model prediction and experimental observation is less than a small value ε. It is calculated as

$$r = \Phi\left[\frac{\sqrt{n_d}(\varepsilon - |\bar{x} - \Theta|)}{s}\right] - \Phi\left[\frac{\sqrt{n_d}(-\varepsilon - |\bar{x} - \Theta|)}{s}\right] \tag{3}$$

where Θ is a single-valued experimentally observed measurement, $\bar{x}$ is the sample mean and s the sample standard deviation of the model predictions, and n_d is the number of data points utilized to calculate $\bar{x}$ and s. The cumulative distribution function of the standard normal distribution is denoted as $\Phi[\cdot]$. In addition to comparing modal frequencies via MRM, mode shape vectors may also be investigated. These comparisons and their results [43] lead to the conclusion that all model predictions are highly correlated to experimental observations in regards to natural frequencies as well as mode shapes, such that the models can be considered validated with high confidence.

B. Probabilistic FEM Analysis

In the current example, plate thickness, Young's modulus, Poison's ratio, and density are modeled as Gaussian random fields with independent, but equal correlation structures along orthogonal axes. A two-dimensional stochastic process was generated for these model inputs using the spectral representation as defined in Eq. (4) via Shinozuka's formulation [42] and the Wiener–Khinchine relations [44]. The Gaussian random field $g_o(x_1, x_2, \phi)$ can be simulated by the following series as N_1 and N_2 approach infinity:

$$g_o(x_1, x_2, \phi) = 2\sum_{k_1=1}^{N_1-1}\sum_{k_2=1}^{N_2-1}[\sqrt{S(\omega_{k_1})S(\omega_{k_2})\Delta\omega_1\Delta\omega_2}\cos(\omega_{k_1}x_1 + \omega_{k_2}x_2 + \phi_{k_1,k_2})] \tag{4}$$

where $\Delta\omega_i = \omega_{u_i}/N_i$, $\omega_{k_i} = k_i\Delta\omega_i$, for $i = 1, 2$. Here ω_{u_i} is the upper cutoff frequency beyond which $S(\omega_{k_i})$ is considered zero. $S(\omega_{k_i})$ is the two-sided power spectral density function of the random field in the i direction and ϕ_{k_1,k_2} an array containing the independent random phase angles uniformly distributed between 0 and 2π. N_i defines the number of terms to be included in the dual summation in the i direction. The random fields in this study utilize the following power spectral density functions: $S(\omega_{k_i}) = 1/4\sigma_i^2 b_i^3 \omega_{k_i}^2 \cdot \exp(-b_i\omega_{k_i})$ for $i = 1, 2$. Here σ_i is the standard deviation of the stochastic process in the i direction and b_i its corresponding correlation distance.

For the random fields considered as inputs to the FEM model of the test article, $b_1 = b_2 = 3$ and $\sigma_1 = \sigma_2 = 1$, where the magnitude of $g_o(x_1, x_2, \phi)$ is scaled after the fact to match the mean and coefficient of variation (COV) of the random field to be simulated. $\omega_{u_1} = \omega_{u_2} = 5\pi$, while $N_1 = N_2 = 35$. Table 1 lists the means and COV used for each of the random fields simulated with Eq. (4).

Temperature uncertainty was included as a random variable uniformly distributed between 65 and 75 °F. The following temperature effect model was constructed via a quadratic regression analysis of data in [45]:

$$F(t) = (-1.151525 \times 10^{-6})t^2 + (2.75775 \times 10^{-5})t + 1.00067 \tag{5}$$

where $F(t)$ is a scale factor for Young's modulus and t is the plate temperature in degrees Fahrenheit.

Repeatedly executing deterministic finite element analyses using realizations of the model inputs provides data for statistical analysis of the model responses. For the example at hand, 500 simulations using 500 realizations of the random inputs were executed; 100 simulations of the healthy model, 100 simulations of the model damaged at bolt 1, 100 simulations of the model damaged at bolt 2, and so on, where a damaged bolt refers to a bolt at 25% nominal

Table 1 Mean and COV values used for random field simulation

	Panel thickness, in./mm	Young's modulus, psi/MPa	Poison's ratio	Density, $(lb/in.^3)/(kg/m^3)$
Mean	0.2458/6.24	9.75E06/6.72E04	0.3	0.000259/7.169
COV	0.02	0.02	0.02	0.02

torque. This damage was simulated analytically by altering the stiffness constants of the spring elements surrounding each bolt location. These five sets of simulations and their corresponding response statistics are used for damage detection. Within each set of 100 FEM simulations, the first 50 simulations are used as the learning or training data set, and the second 50 simulations are used as the testing data set.

C. Damage Detection and State Classification

Figure 4 shows a typical sensor layout, where sensor location 1 is the point of input excitation and stationary, while sensor locations 2, 3, and 4 are the points of sensing and variable. Also shown in Fig. 4 are the locations of the four bolts which hold the test structure in place and are the locations of fastener damage. The hatched areas in Fig. 4 are regions where it is infeasible to place SHM sensors.

From the pool of simulation output of the probabilistic FEM analysis consisting of temporal displacement data, an equivalenced von Mises stress is calculated via Eq. (6) as defined in [42] for each possible sensor location:

$$\sigma_{vM} = \sqrt{\sigma_x^2 - \sigma_x\sigma_y + \sigma_y^2 + 3\tau_{xy}^2} \tag{6}$$

where σ_x, σ_y, and τ_{xy} are the in-plane stress components, which are estimated from the displacement records of the four nearest neighboring nodes. Plane stress conditions are assumed.

From the estimated von Mises stress records at sensor locations S2, S3, and S4, a set of features is extracted. Features are characteristics unique to a signal generated under a given set of parameters. The set of features utilized for this example problem is based in the frequency domain and is extracted via the well-known Welch method [46,47] from the power spectral densities of the signals. With a bin size of 100 measurements and an overlap of 50%, the Welch method produces 51 features each from the signals obtained at piezoelectric sensor locations S2, S3, and S4. Dimensionality reduction is achieved via feature selection. Feature selection provides a subset of N_{opt} features from the m-dimensional feature pool most effective for state classification. In general, the fewer features used in a classifier, the more likely the training set performance will be representative of test set performance [37]. A sequential forward search algorithm [48,49] is used to identify 25 optimal features from the original 153-dimensional feature pool.

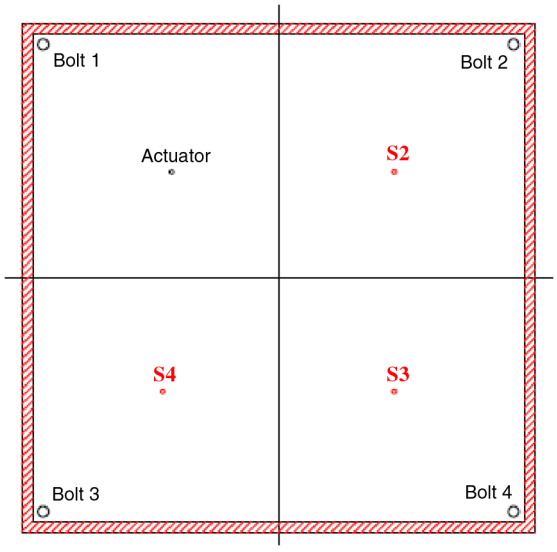

Fig. 4 TPS test plate with typical sensor layout, actuator, and fastener damage locations.

The above defined feature vector is then used for state classification. The state classifier utilized in this work is derived from Bayes decision theory and minimizes the probability of classification error [34]. The discriminant functions, one for each structural state (healthy, damaged at bolt 1, damaged at bolt 2, etc.), are the Mahalanobis distances as given in Eq. (7):

$$d_j(x) = (x - \mu_j)^t \Sigma_j^{-1} (x - \mu_j) \tag{7}$$

where j indexes the structural state, x is a feature vector to be classified, and μ_j and Σ_j are the mean feature vector and covariance matrix of the learning data set of structural state j. The learning data set consists of the first 50 simulations of each structural state. State classification is continued by evaluating each discriminant function for each simulation of the testing data set and assigning the state according to the discriminant function with the smallest value.

Since the Mahalanobis distance in Eq. (7) requires the determination of the inverse of Σ_j it is necessary that the feature covariance matrix be nonsingular. Several techniques are available to ensure the nonsingularity of a matrix [50]. For this specific problem, the covariance matrix can be made nonsingular by adding a small disturbance value (e.g., $0.001a_j$) in the diagonal components (a_j is the value of the jth diagonal component), or by adding a small disturbance value in all components of any particular row or column, or by deleting one or more sets of the learning data.

It has been shown in [44] that the above damage detection algorithm works most efficiently in comparison with damage detection algorithms which utilize other feature types, feature extraction methods, dimensionality reduction schemes, and feature selection algorithms. This damage detection algorithm is then applied to testing data, which consists of the second 50 simulations of each structural state. This yields a classification matrix corresponding to a given sensor layout, from which several performance measures may be estimated. A sample classification matrix is shown in Table 2. Training and testing data sets are reversed to achieve higher fidelity within the classification matrix.

Using the information contained in the classification matrix one can estimate several probabilistic performance measures of a given sensor layout, such as the probability of false alarm (type 1 error), the probability of missed detection (type 2 error), the probability of correct detection (accuracy), and the probability of misdetection (1-accuracy) [51]. P(False Alarm) is defined as the likelihood that the damage detection algorithm classifies a healthy structure as damaged. P(Missed Detection) is the probability that the damage detection method classifies a damaged structure as healthy. Accuracy is measured via P(Correct Detection), which is defined as the probability that the damage detection method will classify a given structure correctly into its proper structural state (i.e. P(classify structure as ω_i|structural state is ω_i)). The compliment of P(Correct Detection) is P(Misdetection). These probabilities can be used to evaluate a given sensor array. The performance measures are expressed as follows:

$$P(\text{Correct Detection}) = \frac{\text{Sum of Diagonal Elements of CM}}{\text{Sum of All Elements of CM}} = P(CD) \tag{8}$$

$$P(\text{False Alarm}) = \frac{\text{Sum of First 4 Elements in Row 5 of CM}}{\text{Sum of All Elements in Row 5 of CM}} = P(\text{TypeI}) \tag{9}$$

Table 2 Sample classification matrix for a given sensor layout

	Classified states				
True states	Damaged 1	Damaged 2	Damaged 3	Damaged 4	Healthy
Damaged 1	1	21	0	0	1
Damaged 2	78	98	0	2	0
Damaged 3	0	1	91	7	1
Damaged 4	0	10	0	89	1
Healthy	0	11	0	1	88

$$P(\text{Missed Detection}) = \frac{\text{Sum of First 4 Elements Column 5 of CM}}{\text{Sum of All Elements in Column 5 of CM}} = P(\text{TypeII}) \tag{10}$$

$$P(\text{Misdetection}) = 1 - P(\text{Correct Detection}) \tag{11}$$

Evaluating Eqs. (8–11) for the classification matrix shown in Table 2 yields the following results: $P(\text{Correct Detection}) = 0.89$; $P(\text{False Alarm}) = 0.12$; $P(\text{Missed Detection}) = 0.033$; $P(\text{Misdetection}) = 0.11$. Repeating the above calculations for different sensor layouts generates different values of the performance measures. Five randomly selected sensor layouts are shown in Fig. 5 and their corresponding performance measures are shown in Table 3. Note that for the five sensor layouts presented, the best sensor layout varies depending on which performance measure is utilized. For example, if maximum $P(CD)$ is desired, sensor configuration SL1 is optimum; however, if minimizing $P(\text{Type1})$ is the objective, sensor layout SL2 performs best. A multi-objective optimization problem with an objective function of the form shown in Eq. (12) may be utilized:

$$f(x) = \alpha \cdot P(CD) + \beta \cdot P(\text{Type1}) + \gamma \cdot P(\text{Type2}) \tag{12}$$

This, however, generates the additional problem of assigning values to α, β, and γ, which may prove to be difficult and depending on what values are chosen may cause the optimal solution to vary significantly.

D. Sensor Placement Optimization

The software package Snobfit [41], programmed in MATLAB [52], is used to solve the optimization formulation given by Eq. (1)

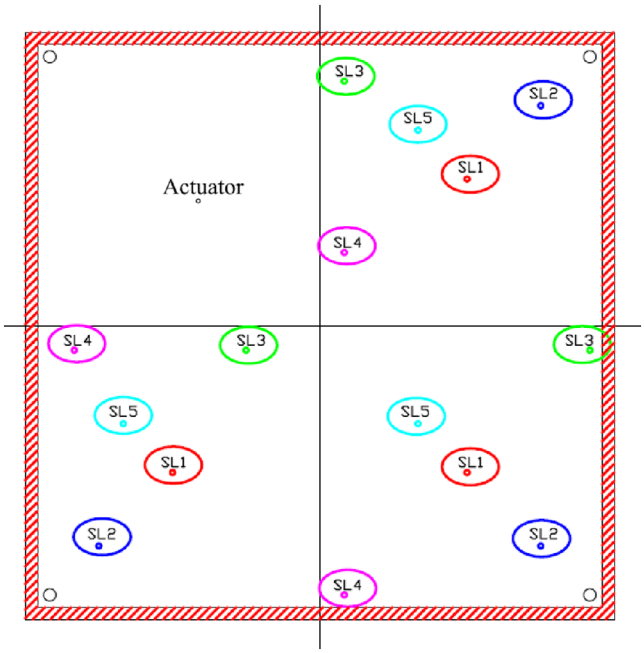

Fig. 5 Five randomly selected sensor layouts.

Table 3 Performance measures corresponding to randomly selected sensor layouts of Fig. 5.

Sensor layout	$P(CD)$	$P(\text{Type1})$	$P(\text{Type2})$
SL1	0.916	0.12	0.0075
SL2	0.860	0.08	0.0050
SL3	0.866	0.12	0
SL4	0.894	0.11	0.0025
SL5	0.872	0.10	0.0075

iteratively. Snobfit is designed specifically to handle the following difficulties that arise with this particular problem:

1) The function values are expensive to evaluate (i.e. obtaining the performance measures for a given sensor layout is computationally intensive).

2) Instead of a function value requested at a point x, only a function value at some nearby point $\tilde{x}$ is returned (the finite mesh size of the FEM models restricts that sensible responses required by the damage detection algorithm to estimate the performance measures are only available at nodal locations).

3) The function values are noisy (due to the finite number of simulations utilized to construct the confusion matrix, there is a finite precision with which the performance measures can be estimated).

4) The objective function may have several local minima.

5) Gradient information is not readily available.

The Snobfit algorithm proceeds as follows to solve Eq. (1). It partitions the bounded box$[u, v]$ into a set of subboxes such that each contains exactly one point. A branching algorithm is utilized for this purpose. Snobfit then builds local quadratic models, around the current best point, x^{best}, and around all other points. Two different types of quadratic models are used: a Hessian fit around the best point, x^{best}, and around all others a quadratic fit using as Hessian a suitable multiple of the Hessian matrix used in the model around x^{best}. The suitable multiple is decided based on the point's distance from x^{best}. The algorithm then suggests a user-specified number of evaluation points to be used in the next iteration of the optimization [41].

The function can be evaluated at these points and other locations for further Snobfit iterations. Because of the fact that the structural FEM model described in Sec. IV.A has a finite fidelity and temporal data is only available at the nodes, the points which Snobfit requests are substituted with the nearest neighboring nodal locations. The damage detection and state classification procedure described in Sec. IV.C is performed for these requested sensor layouts, where vectors u and v confine sensors 2, 3, and 4 to their respective quadrants of the thermal protection system (TPS) component. A natural stopping criterion would be to quit exploration if for a number of iterations no new x^{best} is generated and the accuracy of x^{best} as predicted by Snobfit converges to a reasonably small value. The above defined procedure was carried out for the objective functions listed in the first column of Table 4. Each objective function is tested separately resulting in different candidate solutions shown in Fig. 6. The first three objective functions are single-objective. The fourth and fifth objective functions are of the form shown in Eq. (12), where $\alpha = -0.5$, $\beta = 0.25$, and $\gamma = 0.25$ for the fourth objective function and $\alpha = -0.5$, $\beta = 0.25$, and $\gamma = 5.0$ for the fifth objective function. In addition, the compliment of $P(CD)$, $[1 - P(CD)]$, is utilized in

Table 4 Results for optimal sensor arrays corresponding to different objective functions (units conversion for coordinates of sensors S2, S3 and S4: 1 in. = 25.4 mm)

Objective function $f(y)=$	*Nite*	*Nobj*	Optimal solution coordinates for sensors (in.)			*E*	Corresponding performance measures		
			S2	S3	S4		$P(CD)$	P(Type1)	P(Type2)
$-P(CD)$	71	258	8.75, 6.75	6.0, 3.5	3.5, 0.75	0.0104	0.944	0.13	0.0075
P(Type1)	12	58	7.0, 8.5	11.73, 0.27	5.75, 1.25	0.0426	0.916	0.01	0
P(Type2)	——	——	7.0, 8.5	11.73, 0.27	5.75, 1.25	——	0.916	0.01	0
$-0.5P(CD) + 0.25P$(TypeI) $+0.25P$(TypeII)	55	268	6.75, 8.75	11.60, 0.40	5.75, 1.25	0.0208	0.932	0.03	0.0025
$0.5(1 - P(CD)) + 0.25P$(TypeI) $+5.0P$(TypeII)	44	196	7.0, 8.5	11.73, 0.27	5.75, 1.25	0.0375	0.916	0.01	0

combination with α as the first term of the fifth objective function to adjust the relative importance of each of the three performance measures to ratio of approximately $2:1:1$. This brings the three individual objectives to a comparable scale. The approximate ratio of relative importance of the three performance measures for the fourth objective function is $360:20:1$. Other ratios of relative importance may be achieved by adjusting α, β, and γ. The corresponding results are also shown in Table 4, where *Nite* is the number of Snobfit iterations, *Nobj* is the number of objective function evaluations, and E is the measure of accuracy of the quadratic model at the optimal solution as estimated by Snobfit. The coordinates given are with respect to the bottom left corner of the plate. The results are visually presented in Fig. 6.

From Table 4 and Fig. 6 it can concluded that although the solution varies for different objective functions, the optimal sensor arrays corresponding to objective functions 2 through 5 are virtually identical. Additionally, it was observed during Snobfit's iterations that the optimal solutions to objective functions 2 through 5 was robust and insensitive to small changes in the independent variables (i.e. shifting sensors S2, S3, and/or S4 by less than 0.25 in. in any direction, did not significantly alter the performance measures). However, the solution to the first objective function, $f(x)=-P(CD)$, was very sensitive with respect to small changes in the independent variables (i.e. shifting sensors S2, S3, and/or S4 by less than 0.25 in. in any direction, significantly degraded the performance measures).

While optimizing the third objective function, $f(x)=-P$(Type2), several sensor configurations produced probabilities of missed detection of zero percent, creating multiple optimal solutions. Among these, the solution $[S2(7.0, 8.5); S3(11.73, 0.27); S4(5.75, 1.25)]$ {in units of inches; the corresponding values in SI units (m) are $[S2(0.18, 0.22); S3(0.30, 0.007), S4(0.146, 0.032)]$} is reported here as the optimal solution for the third objective function, since it also optimizes objectives 2 and 5.

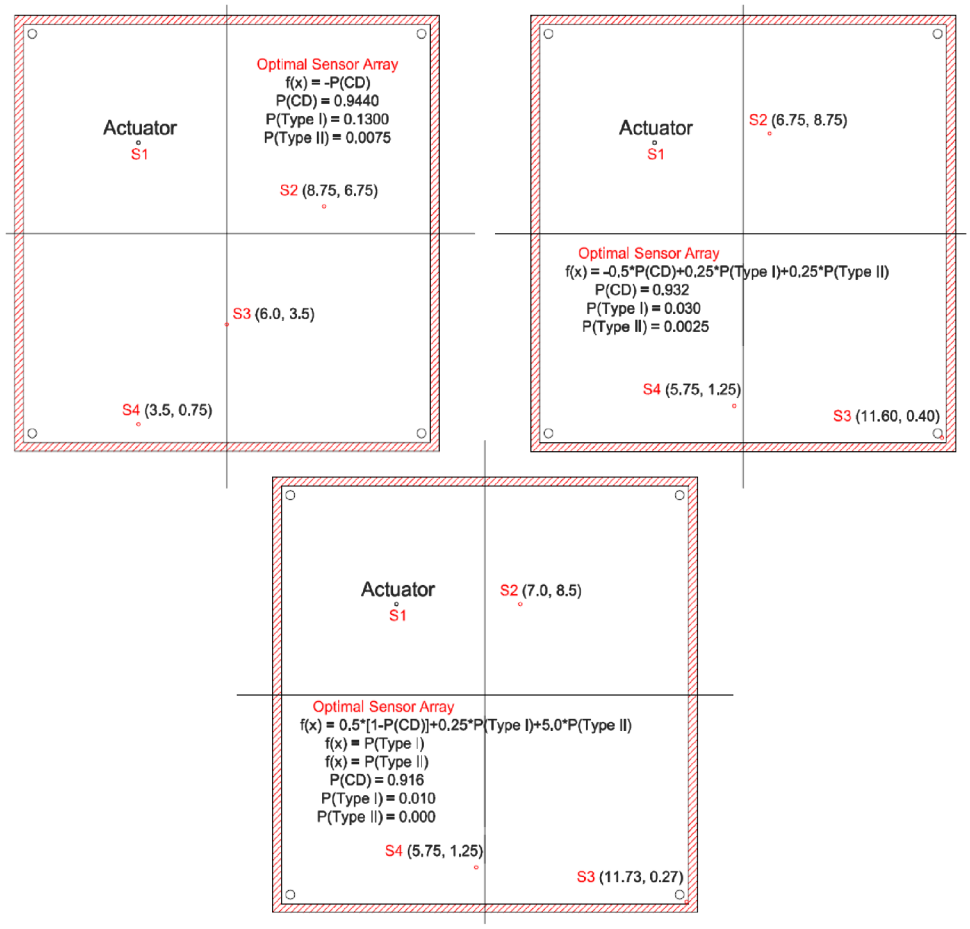

Fig. 6 Optimal sensor arrays for different objective functions. (Coordinates of S2, S3, and S4 are shown in units of inches. Coordinate origin is the left bottom corner of the plate. Units conversion: 1 in. = 25.4 mm).

V. Conclusions

A methodology for SPO under uncertainty is developed in this paper. The method consists of four components: 1) structural simulation and model validation, 2) probabilistic analysis, 3) damage detection, and 4) SPO. The methodology is applied to the optimization of the sensor array of a SHM system for a simplified TPS component. The methodology is implemented in the context of vibration-based sensing, and specific algorithms within the above four components need to be tailored for other sensing approaches. Thus the limitations of vibration-based approaches (e.g., inability to apply to barely visible impact damage) are also present in the detailed algorithms discussed in this paper. However, the proposed framework and the probabilistic analysis approach are quite general, and can be combined with other sensing approaches and performance criteria for other applications.

Further work is required in regards to validating this methodology with experimental data. An additional investigation is necessary to determine the optimum number of sensors. In this paper the number of sensors was fixed; only their coordinates were design variables. It is reasonable to assume that as the number of sensors distributed across the structure increases, the estimated SHM performance measures improve. However, due to weight penalties associated with additional sensors, as well as complexity constraints with respect to the amount of data acquired by the sensing system that requires processing (and therefore processing power), the number of sensors applied to the structure must be minimum. In addition, future work needs to incorporate sensor reliability and redundancy into the optimization. This paper included thermal analysis, however, the sensors were assumed to be unaffected by temperature. Issues such as sensor performance and degradation, and the performance of damage detection algorithms, under various environmental and operating conditions need to be addressed in future work.

Acknowledgments

This research is funded partly by the National Science Foundation through the Integrative Graduate Education and Research Training doctoral program in Reliability and Risk Engineering and Management at Vanderbilt University, and partly by the U.S. Air Force Research Laboratory (project monitor: Mark Derriso) through subcontract to Anteon Corporation. The authors gratefully acknowledge this support. The authors also gratefully acknowledge valuable discussions with Chris Pettit at the U.S. Naval Academy, Steven Olson at University of Dayton Research Institute, and Martin DeSimio at Alliant Techsystems, Inc., in the development of the proposed methodology and their help with finite element models and model validation experiments. The valuable help provided by Xiaomo Jiang at Vanderbilt University is also gratefully acknowledged.

References

[1] Shkarayev, S., Krashantisa, R., and Tessler, A., "An Inverse Interpolation Method Utilizing In-Flight Strain Measurements for Determining Loads and Structural Response of Aerospace Vehicles," *Proceedings of the Third International Workshop on Structural Health Monitoring*, Stanford, CA, 2001.

[2] Hiramoto, K., Doki, H., and Obinata, G., "Optimal Sensor/Actuator Placement for Active Vibration Control Using Explicit Solution of Algebraic Riccati Equation," *Journal of Sound and Vibration*, Vol. 229, No. 5, 2000, pp. 1057–1075. doi:10.1006/jsvi.1999.2530

[3] Abdullah, M., Richardson, A., and Hanif, J., "Placement of Sensor/Actuators on Civil Structures Using Genetic Algorithms," *Earthquake Engineering and Structural Dynamics*, Vol. 30, No. 8, 2001, pp. 1167–1184. doi:10.1002/eqe.57

[4] Yan, Y. J., and Yam, L. H., "Optimal Design of Number and Locations of Actuators in Active Vibration Control of a Space Truss," *Smart Materials and Structures*, Vol. 11, No. 4, 2002, pp. 496–503. doi:10.1088/0964-1726/11/4/303

[5] Simpson, M. T., and Hansen, C. H., "Use of Genetic Algorithms to Optimize Vibration Actuator Placement or Active Control of Harmonic Interior Noise in Cylinder with Floor Structure," *Journal of Noise Control Engineering*, Vol. 44, No. 4, 1996, pp. 169–184.

[6] Peng, F., "Actuator Placement Optimization and Adaptive Vibration Control of Plate Smart Structures," *Journal of Intelligent Material Systems and Structures*, Vol. 16, No. 3, 2005, pp. 263–271. doi:10.1177/1045389X05050105

[7] Demetriou, M. A., "Integrated Actuator-Sensor Placement and Hybrid Controller Design of Flexible Structures Under Worst Case Spatiotemporal Disturbance Variations," *Journal of Intelligent Material Systems and Structures*, Vol. 15, No. 12, 2004, pp. 901–921. doi:10.1177/1045389X04045152

[8] Guo, H. Y., Zhang, L., Zhang, L. L., and Zhou, J. X., "Optimal Placement of Sensors for Structural Health Monitoring Using Improved Genetic Algorithms," *Smart Materials and Structures*, Vol. 13, No. 3, 2004, pp. 528–534. doi:10.1088/0964-1726/13/3/011

[9] Spanache, S., Escobet, T., and Trave-Massuyes, L., "Sensor Placement Optimization Using Genetic Algorithms," *Proceedings of the 15th International Workshop on Principles of Diagnosis*, Carcassonne, France, 2004.

[10] Berry, J. W., Hart, W. E., Phillips, C. A., Uber, J. G., and Watson, J. P., "Sensor Placement in Municipal Water Networks with Temporal Integer Programming Models," *Journal of Water Resources Planning and Management*, Vol. 132, No. 4, 2006, pp. 218–224. doi:10.1061/(ASCE)0733-9496(2006)132:4(218)

[11] Kumar, A., Kansal, M. L., and Arora, G., "Discussion of Detecting Accidental Contaminations in Municipal Water Networks," *Journal of Water Resources Planning and Management*, Vol. 124, No. 4, 1998, pp. 308–310.

[12] Watson, J. P., Greenberg, H. J., and Hart, W. E., "A Multiple-Objective Analysis of Sensor Placement Optimization in Water Networks," *Proceedings of the World Water and Environmental Resources Congress*, Salt Lake City, UT, 2004.

[13] Guestrin, C., "Placement, Coordination and Tasking of Static and Mobile Sensor Networks," www.cs.ucsb.edu/~suri/Workshop06/guestrin.pdf [retrieved 10 Sept. 2006].

[14] Ganesan, D., Cristescu, R., and Beferull-Lozano, B., "Power-Efficient Sensor Placement and Transmission Structure for Data Gathering Under Distortion Constraints," *ACM Transactions on Sensor Networks*, Vol. 2, No. 2, May 2006, pp. 155–81.

[15] Krause, A., Gupta, A., Guestrin, C., and Kleinberg, J., "Near-Optimal Sensor Placement: Maximizing Information While Minimizing Communication Cost," *Proceedings of the Fifth International Conference on Information Processing in Sensor Networks*, Nashville, TN, 2006.

[16] Jourdan, D. B., and de Weck, O. L., "Layout Optimization for a Wireless Sensor Network Using a Multi-Objective Genetic Algorithm," *Proceedings of the IEEE 60th Vehicular Technology Conference*, Los Angeles, CA, 26–29 Sept. 2004.

[17] Li, D., Li, H., and Fritzen, C. P., "A New Sensor Placement Algorithm in Structural Health Monitoring," *Proceedings of the Third European Workshop on Structural Health Monitoring*, Granada, Spain, 2006.

[18] Gao, H., and Rose, J. L., "Ultrasonic Sensor Placement Optimization in Structural Health Monitoring Using Evolutionary Strategy," *Proceedings of the AIP Conference on Quantitative Nondestructive Evaluation*, Vol. 820, 2006, pp. 1687–1693.

[19] Dhillon, S. S., Chakrabarty, K., and Iyengar, S. S., "Sensor Placement for Grid Coverage Under Imprecise Detection," *Proceedings of the International Conference on Information Fusion*, Annapolis, MD, 2002.

[20] Parker, D. L., and Frazier, W. G., "Experimental Validation of Optimal Sensor Placement Algorithms for Structural Health Monitoring," *Proceedings of the Third European Workshop on Structural Health Monitoring*, Granada, Spain, 2006.

[21] Edwins, D. J., *Modal Testing: Theory, Practice and Application*, 2nd ed., Research Studies Press, Philadephia, PA, 2000.

[22] Rebba, R., and Mahadevan, S., "Probabilistic Assessment of CAE Models," Paper No. 2006-01-0226, SAE 2006 World Congress, Detroit, MI, 2006.

[23] Haldar, A., and Mahadevan, S., *Reliability Assessment Using Stochastic Finite Element Analysis*, Wiley, New York, 2000.

[24] Huang, S., "Simulation of Random Processes Using Karhunen–Loeve Expansion," Ph.D. Dissertation, National Univ. of Singapore, Republic of Singapore, 2001.

[25] Tedesco, J. W., McDougal, W. G., and Ross, C. A., *Structural Dynamics: Theory and Application*, Addison Wesley Longman, Reading, MA, 1999.

[26] Sakamoto, S., and Ghanem, R., "Polynomial Chaos Decomposition for the Simulation of Non-Gaussian Nonstationary Stochastic Processes,"

Journal of Engineering Mechanics, Vol. 128, Feb. 2002, pp. 190–201. doi:10.1061/(ASCE)0733-9399(2002)128:2(190)

[27] Deodatis, G., and Micaletti, R. C., "Simulation of Highly Skewed Non-Gaussian Stochastic Processes," *Journal of Engineering Mechanics*, Vol. 127, Dec. 2001, pp. 1284–1295.

[28] Corbin, M., Hera, A., and Hou, Z., "Location Damage Regions Using Wavelet Approach," http://wusceel.cive.wustl.edu/asce.shm/pdfs/corbin_hera_hou.pdf [retrieved 29 Oct. 2003].

[29] Ching, J., and Beck, J. L., "Bayesian Analysis of the Phase 2 IASC–ASCE Structural Health Monitoring Experimental Benchmark Data," *Journal of Engineering Mechanics*, Vol. 130, No. 10, 2004, pp. 1233–1244. doi:10.1061/(ASCE)0733-9399(2004)130:10(1233)

[30] Doebling, S. W., Farrar, C. R., Prime, M. B., and Shevitz, D. W., "Damage Identification and Health Monitoring of Structures and Mechanical Systems from Changes in Their Vibration Characteristics: A Literature Review," Los Alamos National Lab., Rept. LA-13070-MS, Los Alamos, NM, 1996.

[31] Banks, H. T., Joyner, M. L., Bincheski, B., and Winfree, W. P., "Real Time Computational Algorithms for Eddy-Current-Based Damage Detection," *Inverse Problems*, Vol. 18, 2002, pp. 795–823. doi:10.1088/0266-5611/18/3/318

[32] Pines, D. J., "The Use of Wave Propagation Models for Structural Damage Identification," *Structural Health Monitoring: Current Status and Perspectives*, Stanford Univ., Palo Alto, CA, 1997, pp. 665–677.

[33] Staszewski, W. J., Boller, C., Grondel, S., Biemans, C., O'Brien, E., Delebarre, C., Tomlinson, G. R., "Damage Detection Using Stress and Ultrasonic Waves," *Health Monitoring of Aerospace Structures*, edited by W. J. Staszewski, C. Boller, and G. R. Tomlinson, Wiley, Hoboken, NJ, 2004.

[34] Duda, R. O., Hart, P. E., and Stork, D. G., *Pattern Classification*, 2nd ed., Wiley, New York, 2001.

[35] Padula, L. S., and Kincaid, R. K., "Optimization Strategies for Sensor and Actuator Placement," NASA TM-1999-209126, April 1999.

[36] Padula, L. S., and Kincaid, R. K., "Optimal Sensor/Actuator Locations for Active Structural Acoustic Control," *Proceedings of the 39th AIAA/ASME/ASCE/AHS/ASC Structures, Dynamics and Materials Conference*, Long Beach, CA, 20–23 April 1998.

[37] DeSimio, M., Miller, I., Derriso, M., Brown, K., and Baker, M., "Structural Health Monitoring Experiments with a Canonical Element of an Aerospace Vehicle," *Proceedings of the 2003 IEEE Aerospace Conference*, Big Sky, MT, 2003.

[38] Raich, A. M., and Liszkai, T. R., "Multi-Objective Genetic Algorithm Methodology for Optimizing Sensor Layouts to Enhance Structural Damage Detection," *Proceedings of the Fourth International Workshop on Structural Health Monitoring*, Stanford, CA, 2003.

[39] Padula, L. S., and Kincaid, R. K., "Aerospace Applications of Integer and Combinatorial Optimization," NASA TM-110210, Oct. 1995.

[40] Spall, J. C., "An Overview of the Simultaneous Perturbation Method for Efficient Optimization," *Johns Hopkins APL Technical Digest*, Vol. 19, No. 4, 1998, pp. 482–492.

[41] Huyer, W., and Neumaier, A., "SNOBFIT: Stable Noisy Optimization by Branch and Fit," *ACM Transactions on Mathematical Software* (submitted for publication), http://www.mat.univie.ac.at/~neum/software/snobfit/ [retrieved 25 May 2004].

[42] Ansys, ANSYS Release 9.0 Documentation, ANSYS, 2004.

[43] Olson, S., DeSimio, M., and Derriso, M., "Fastener Damage Estimation in a Square Aluminum Plate," *Structural Health Monitoring Journal*, Vol. 5, No. 2, 2006, pp. 185–193.

[44] Guratzsch, R. F., "Sensor Placement Optimization for Structural Health Monitoring Systems of Hot Aerospace Structures," Ph.D. Dissertation, Vanderbilt Univ., Nashville, TN, 2007.

[45] Shinozuka, M., and Deodatis, G., "Simulation of Stochastic Processes by Spectral Representation," *Applied Mechanics Reviews*, Vol. 44, No. 4, 1991, pp. 191–204. doi:10.1115/1.3119501

[46] VanMarcke, E., *Random Fields: Analysis and Synthesis*, MIT Press, Cambridge, MA, 1983.

[47] The Royal Aeronautical Society, *Material Properties Handbook: Volume 1 Aluminum Alloys*, NATO Advisory Group for Aerospace Research and Development, London, 1966.

[48] Oppenheim, A. V., and Schafer, R. W., *Digital Signal Processing*, Prentice–Hall, Upper Saddle River, NJ, 1975.

[49] Welch, P. D., "The Use of Fast Fourier Transform for the Estimates of Power Spectra: A Method Based on Time Averaging Over Short, Modified Periodograms," *IEEE Transactions on Audio and Electroacoustics*, Vol. 15, June 1967, pp. 70–73. doi:10.1109/TAU.1967.1161901

[50] Somol, P., Pudil, P., Novovicova, J., and Paclik, P., "Adaptive Floating Search Methods in Feature Selection," *Pattern Recognition Letters*, Vol. 20, Nos. 11–13, 1999, pp. 1157–1163.

[51] Jain, A., and Zongker, D., "Feature Selection: Evaluation, Application and Small Sample Performance," *IEEE Transactions on Pattern Analysis and Machine Intelligence*, Vol. 19, No. 2, 1997, pp. 153–158. doi:10.1109/34.574797

[52] MATLAB, MathWorks, Service Pack 2, Ver. 7.0.4.365 (R14), 29 Jan. 2005.

C. Cesnik
Associate Editor